An improved bias correction for SSMIS: Assimilation Assessment

Anna Booton, William Bell, Edward Pavelin

Met Office, FitzRoy Road, Exeter, UK

The Special Sensor Microwave Imager Sounder (SSMIS) instruments flying on the Defense Meteorological Satellite Program's (DMSP) platforms are known to suffer calibration anomalies that manifest as complex biases. Despite physically based corrections being employed, significant residual biases remain that hamper the successful exploitation of SSMIS radiance information within numerical weather prediction (NWP) models. However, an improved, complimentary bias correction technique has been developed and demonstrated in offline studies to have great potential for effectively mitigating these difficult orbital biases. The new technique uses a Fourier series in the orbital angle to parameterize the instrument biases, with the coefficients tuned within the Met Office's variational bias correction scheme.

A series of assimilation experiments independently utilizing the SSMIS observations from the temperature sounding, humidity sounding and imaging channels are assessed. The effectiveness of the bias correction technique is illustrated through the examination of observation-minus-background field differences, in which the measurement uncertainties of the F-17, F-18, and F-19, SSMIS brightness temperatures are now found to be comparable with those of the AMSU instruments. Furthermore, assimilation of the improved data is shown to provide positive impact on forecast quality.

Introduction

The Special Sensor Microwave Imager Sounder (SSMIS) instruments provide temperature and humidity soundings as well as imager data, measuring radiances from the surface into the mesosphere. Unfortunately, the instruments suffer from calibration anomalies that manifest as complex orbital biases, making the data difficult to utilize. Physically based corrections have been successful in reducing the biases from ~1 K to ~0.3 K. However, they should ideally be reduced further still to avoid degradation to numerical weather prediction (NWP) analyses and realize benefit when assimilated.

The nature of the calibration anomalies may be elucidated when comparing the observed brightness temperatures (O) with those from NWP model backgrounds (B). Such analysis can be employed to expose the orbital biases affecting the SSMIS datas. For example, maps showing the brightness temperature departures (O-B) presented in Figure 1 clearly reveal that the ascending passes are warmer than those descending. This is emphasised in the accompanying histograms in which a bimodal, rather than Gaussian distribution is seen.

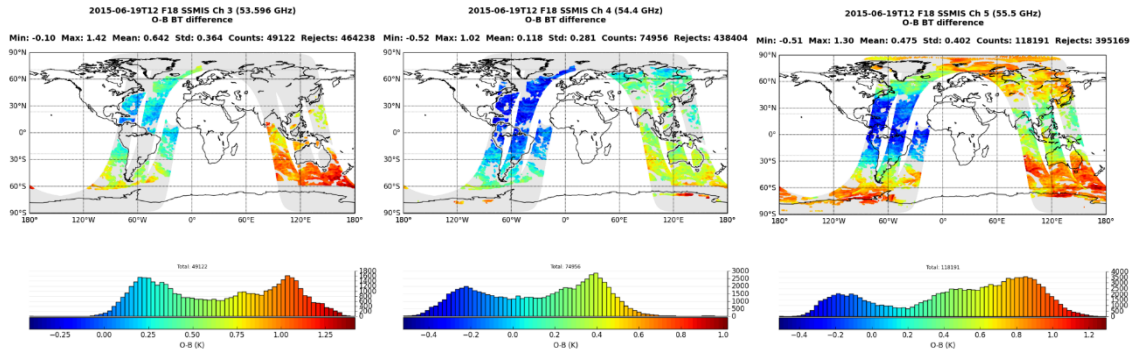

Figure 1: (O-B) brightness temperature departures for F-18 SSMIS for the 53.6 GHz (Ch 3), 54.4 GHz (Ch 4), and 55.5 GHz (Ch 5) channels, on 19 June 2015 12Z. The cooler descending and warmer ascending passes highlight the orbital bias.

The structure and stability of these residual biases are particularly apparent when the (O-B) departures are assessed with respect to the satellite's orbital angle[1], Φ, as in Figure 2. Here, F18 SSMIS O-B brightness temperature data are collected with respect to Φ over a seven day period (28 cycles) and the data are presented as a 2*D* histogram of brightness temperature departures versus Φ. The large amplitude of the peak-to-peak biases, typically 1 K, is also noted.

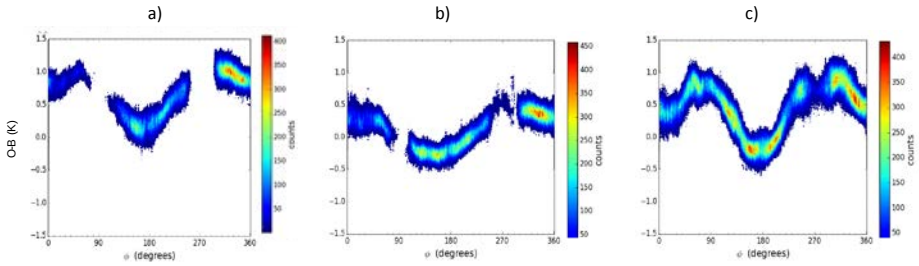

Figure 2: 2D histograms of (O B) brightness temperature departure plotted w.r.t Φ for data accumulated for F18 SSMIS a) 53.6 GHz (Ch 3), b) 54.4 GHz (Ch 4), and c) 55.5 GHz (Ch 5), over 28 cycles from 17th June – 24th June 2015. The peak-to-peak biases are approximately ~1.0 K, ~0.7 K and ~1.2 K in (a-c) respectively. 0° Φ approximately coincides with the equator during these dates.

The Orbital Bias Correction: A Fourier Series Approach

We have developed a new orbital bias correction technique whereby a complement of Fourier component bias predictors are used to generate a Fourier series 'fit' that characterises the form of the bias along the satellite track. The 'correcting fit' is then subtracted from the observed brightness temperatures, thus mitigating the bias and obtaining the corrected brightness temperatures (C).

The correction applied is given by

$$\Delta T_B = \sum_{i=0}^{N} a_i \cos(i\phi) + b_i \sin(i\phi)$$

[1] The satellite orbital angle being the angle along the orbital plane (i.e. about the satellite's track) as referenced from the intersection of the satellite's ascending node and the ecliptic plane.

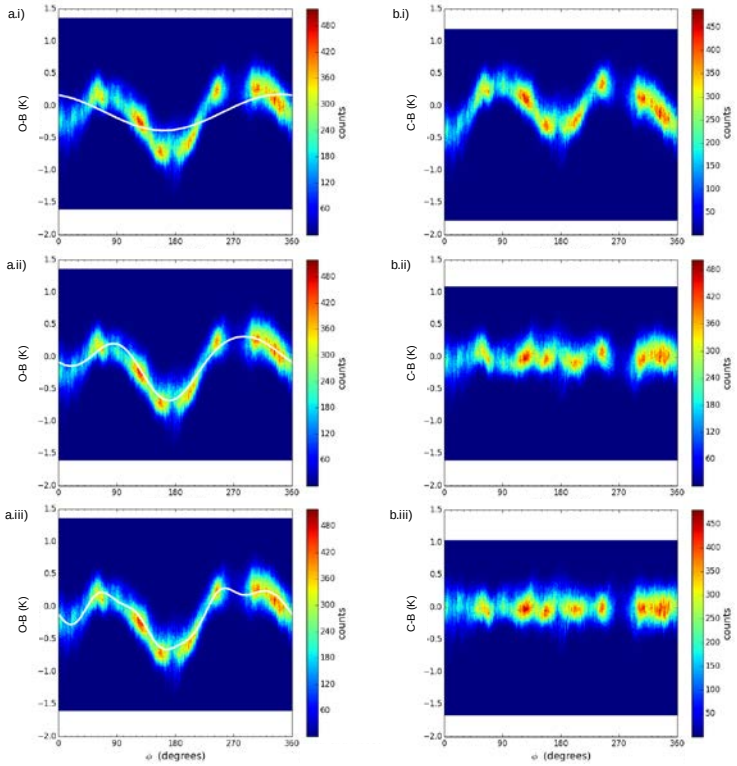

Figure 3: 2D histograms of a) (O-B) and b) (C-B) brightness temperature departure plotted w.r.t. Φ for data accumulated for F18 SSMIS 57 GHz (Ch 6), over 28 cycles from 17th June – 24th June 2015. Fourier series fits to (O-B)'s are over-plotted in white, as calculated for N=1, 3, and 6 in (i)-(iii) respectively. As N increases the 'fit' is improved and the residual bias is progressively mitigated.

where there are N sets of cosinusoidal bias predictors, $\cos(i\Phi)$, and their associated coefficients, a_i, and N sets of sinusoidal bias predictors, $\sin(i\Phi)$, and coefficients, b_i. This has the advantage that by utilizing a larger set of Fourier component predictors enables the more complex bias structures to be fitted. This is illustrated in Figure 3 in which an increasing number (N=1, N=3 and N=6) of Fourier bias predictors have been used to correct the raw (O-B) departures. The residual bias is significantly reduced when twelve predictors (N=6) are utilized, as shown in (c.iii), as the structure is reduced to near zero.

Applying the orbital correction in-conjunction with a cross-scan positional correction proved successful in mitigating the biases. This can be seen in Figure 4 as the structure in the (C-B) brightness temperature departures have been significantly reduced from the raw departures considered in Figure 2.

Examining the post-bias correction (C-B) brightness temperature departure maps, Figure 5,

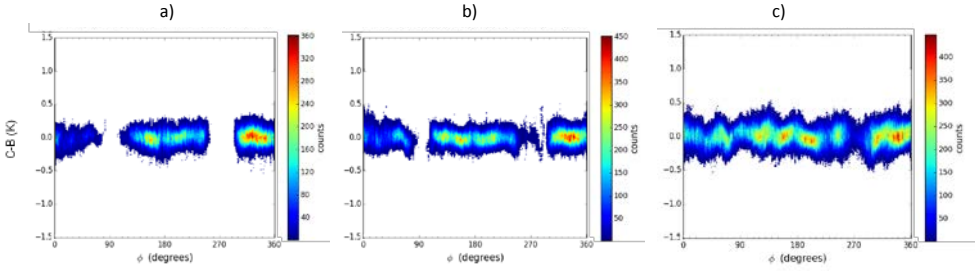

Figure 4: 2D histograms of (C B) brightness temperature departure plotted w.r.t Φ for data accumulated for F18 SSMIS a) 53.6 GHz (Ch 3), b) 54.4 GHz (Ch 4), and c) 55.5 GHz (Ch 5), over 28 cycles from 17th June – 24th June 2015.

(corresponding to those in Figure 1) we note that they no longer exhibit the ascending/descending bias, and the histograms show the departure distributions to be approximately Gaussian.

Similar results are obtained when the correction is applied to the other channels, and to the F17 (Figure 6) and F19 (Figure 7) instrument data.

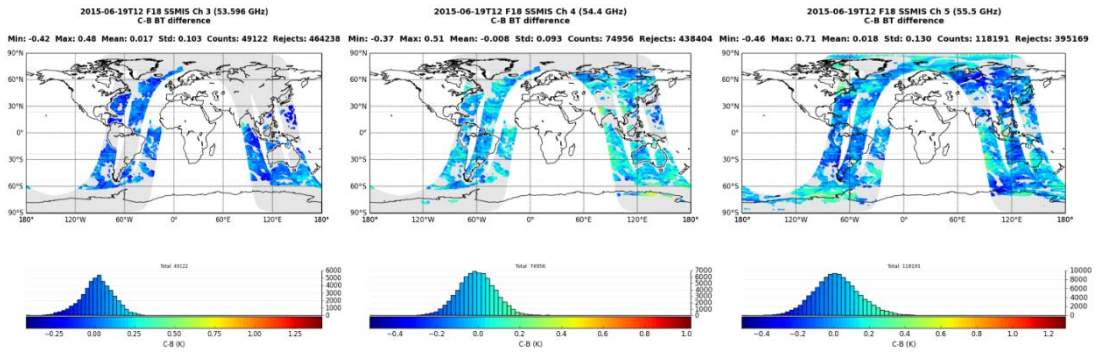

Figure 5: Post-bias correction (C-B) brightness temperature departure maps for F18 SSMIS lower atmosphere temperature sounding channels, 3 (53.6 GHz), 4 (54.4 GHz) and 5 (55.5 GHz).

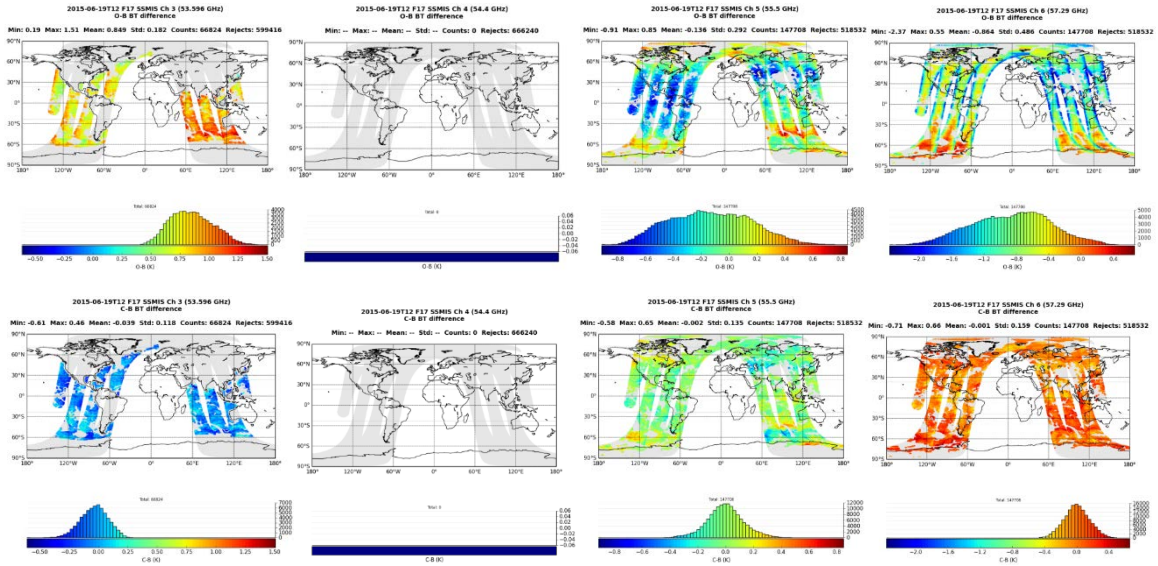

Figure 6: top) Raw (O-B) and bottom) post-bias correction (C-B) brightness temperature departure maps for F17 SSMIS lower atmosphere temperature sounding channels, 3 (53.6 GHz), 4 (54.4 GHz), 5 (55.5 GHz) and 6 (57.3 GHz).

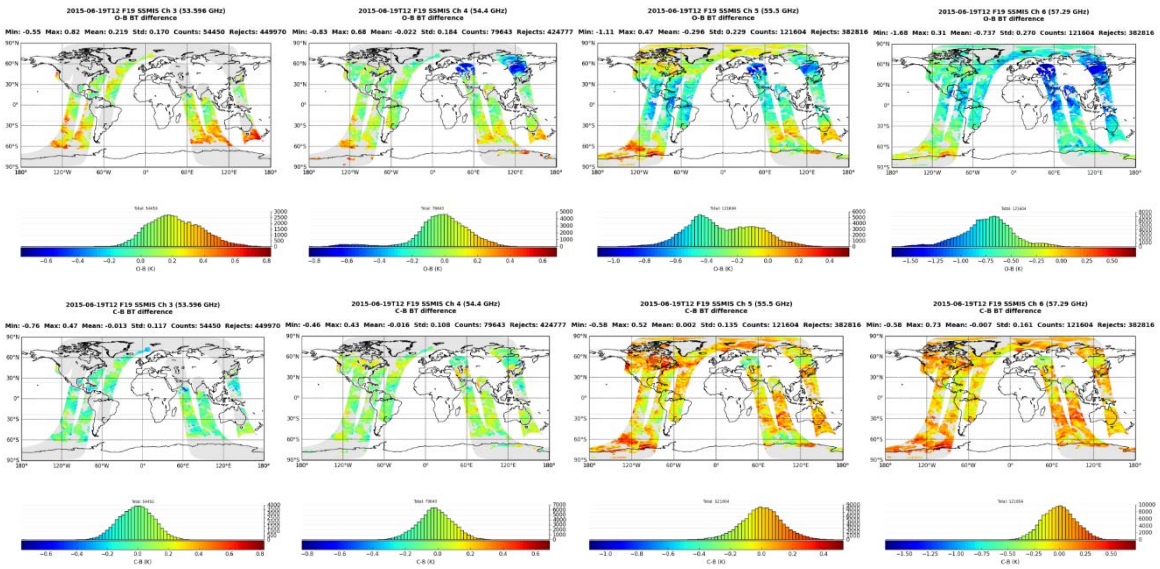

Figure 7: top) Raw (O-B) and bottom) post-bias correction (C-B) brightness temperature departure maps for F19 SSMIS lower atmosphere temperature sounding channels, 3 (53.6 GHz), 4 (54.4 GHz), 5 (55.5 GHz) and 6 (57.3 GHz).

The correction technique was found to work equally well when applied to the humidity and imager channels, although fewer Fourier bias predictors were used. The humidity and imager channels are less susceptible to the strong orbital biases, as characterised by the relatively featureless (O-B) brightness temperature histograms in Figure 8 (b-c). Hence, a Fourier Series correction of fewer components is more appropriate. Furthermore, only sea-clear observations are assimilated from these channels, and so fewer components also constrain the fit in the regions where surface observations are rejected. Consequently, twelve predictors (N=6) were used for correcting the temperature sounding channels (Figure 8 (a)) whilst four orbital predictors and a constant (N=2) were used when correcting the humidity sounding (Ch 9-11) (Figure 8 (b)) and imager (Ch 12-16) data (Figure 8 (c)).

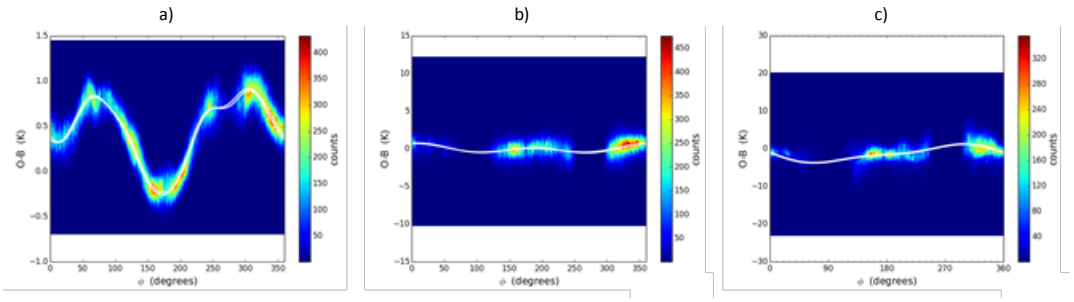

Figure 8: 2D histograms of (O-B) brightness temperature departure plotted w.r.t Φ for data accumulated for F18 SSMIS F18 a) temperature sounding channel 6 (57.3 GHz), b) humidity sounding channel 11 (183±1 GHz) and c) imager channel 16 (37V GHz), over 28 cycles from 17th June – 24th June 2015. The envelope of the (a) 12 component (N=6) and (b-c) 4 component (N=2) Fourier series corrections, ΔT_B, are over-plotted in white.

Evolution of the predictor coefficients

The nature of the orbital bias has a seasonal dependency such that the (O-B) bias structure evolves with time. Therefore, the new correction technique has been implemented within our variational bias correction data assimilation scheme, VarBC. This is accomplished by updating the magnitude of the bias predictor coefficients, here a_i and b_i, at each assimilation cycle. The slow evolution in the

magnitude of these coefficients, as shown in Figure 9, indicates that the bias correction is stable.

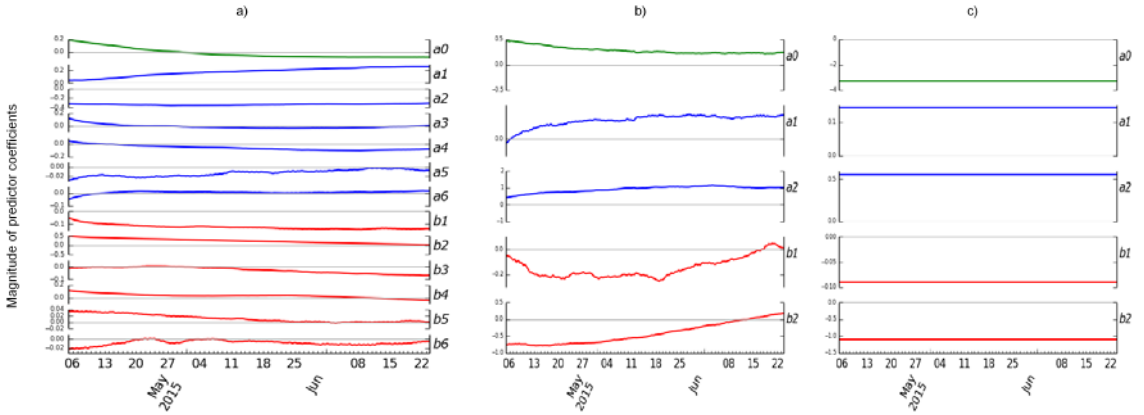

Figure 9: Evolution of the orbital bias predictor coefficients, a_i and b_i, over a three month period for F18 a) temperature sounding Ch 6 (57.3 GHz), b) humidity sounding Ch 11 (183±1 GHz) and c) imager channel 16 (37V GHz). The coefficients' values stabilize after an initial spin-up period.

Assimilation Experiments

The impact of utilising F17 and F18 SSMIS temperature sounding (Ch 2-7, 23,24), humidity sounding (Ch 9-11) and imager (Ch 12-16) data were assessed through three assimilation experiments. The experiments introduced the data into full observing system trials, covering the period of 24th June – 15th July 2014. A 'unified' temperature-humidity-imager experiment (Ch 2-7, 9-16,23-24) was also run for the slightly shorter duration of 24th June – 9th July 2014.

The standard deviation of the innovations (C-B) for key SSMIS channels were compared with those of equivalent channels on the AMSU, ATMS, MHS, SAPHIR and AMSR2 microwave instruments. It should be noted that F19 SSMIS, Megha-Tropiques SAPHIR and GCOM1-W1 AMSR2 data were not included in the experiments described above. Instead, innovation statistics relating to these instruments were derived from a subsequent experiment assimilating a suite of new satellite instrument data. The results are included as an approximate comparison.

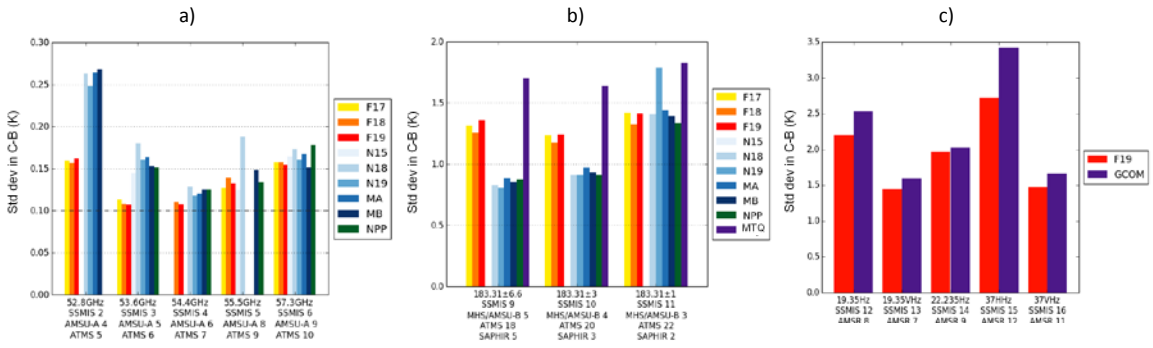

Figure 10: Comparisons of innovation (C-B) departures for key tropospheric SSMIS a) temperature sounding, b) humidity sounding and c) imager channels, with closest-equivalent channel selections from other MW instruments.

The temperature sounding statistics, Figure 10 (a), indicate the assimilated SSMIS data to be of comparable or better quality than the equivalent AMSU-A and ATMS channels. The SSMIS humidity data departures, Figure 10 (b), are however larger than those of their MHS/AMSU-B counterparts, although are better than SAPHIR. The SSMIS imager data departures, Figure 10 (c), are better than

for AMSR2.

Assimilation of the SSMIS temperature sounding information led to a general improvement in the background fits (first guess departures, C-B) to the AMSU and ATMS observations, as in Figure 11. The temperature soundings, (a), were particularly improved in the mid-troposphere and stratospheric channels, being more mixed around the tropopause, whilst all the microwave water vapour observations, (b), showed improvements.

Verification

The impact on a range of verification measures is shown in Figure 12. Consistent small improvements are seen in most verification metrics in each of the individual experiments. The introduction of the temperature sounding data, (Figure 12 a), provided the most positive benefit in both the northern and southern hemispheres. Smaller impacts were delivered in the humidity experiment, (Figure 12 b), and although results were more mixed in the imager experiment, (Figure 12 c), consistent benefit is found in the southern hemisphere. However, the greatest impact arises in the unified trial, (Figure 12 d), in which the benefits seen in the individual experiments appear to combine, delivering stronger positive impact in the southern hemisphere than was seen in the separate components.

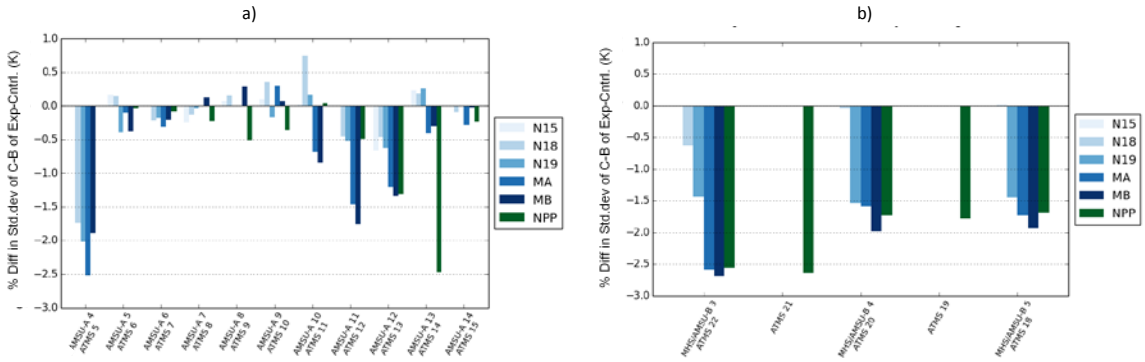

Figure 11: Background fits (C-B) to AMSU and ATMS a) temperature and b) humidity sounding channels on the NOAA 15 - NOAA 19 (N15-19), Metop A - Metop B (MA-B) and NPP satellites.

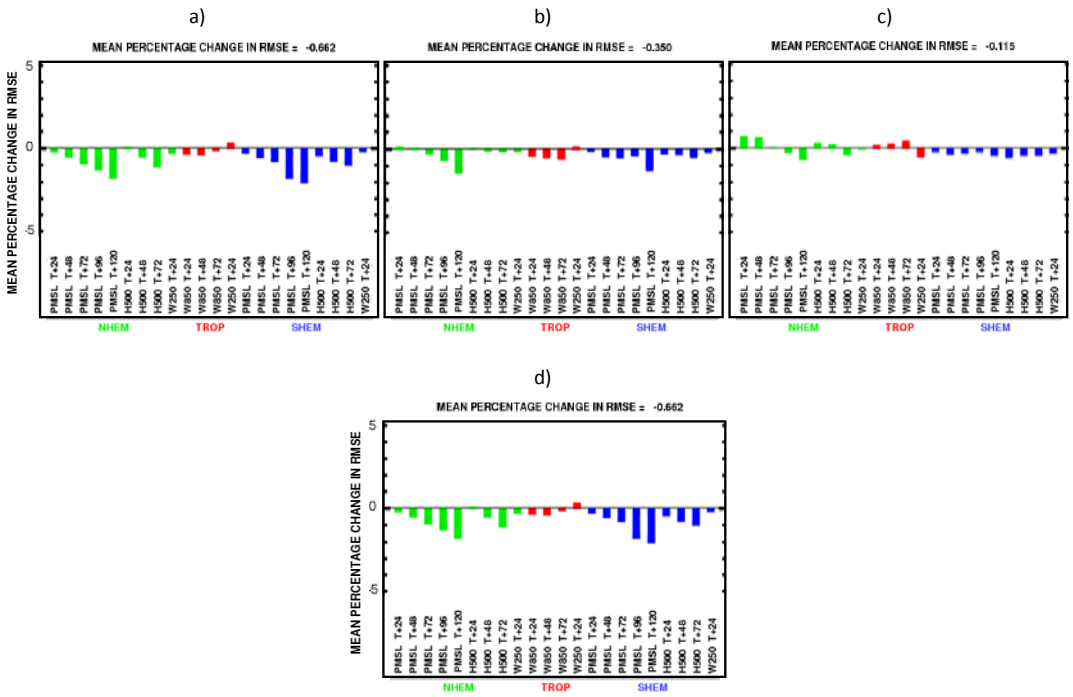

Figure 12: Verification vs MO analysis for the a) temperature sounding b) humidity sounding, c) imager and d) unified assimilation experiments, wrt no-SSMIS control.

More detailed analysis of the southern hemisphere verification, for which the more significant impacts were found, is presented in Figure 13. Here, the differences in RMS errors of the short-range (forecast-analysis) fields from the suite of experiments are compared with those from the no-SSMIS control. Assessment of the temperature profiles (Figure 13 a) shows the information assimilated in the temperature sounding experiment provided consistent benefit throughout every profile, at each forecast period. Indeed, this is the case for the other diagnostics considered (Figure 13 b - d) as well. However, as found in the Figure 12, it is the combination of information from the temperature, humidity and imager channels provides the best impact, particularly in the mid-troposphere (most negative RMSE differences, pink curve). The relative humidity profiles (Figure 13 b) are generally improved although they show apparent degradation at 850hPa. The geopotential heights show improvements throughout the whole profile, as do the wind profiles, with the unified experiment once again showing the best benefit.

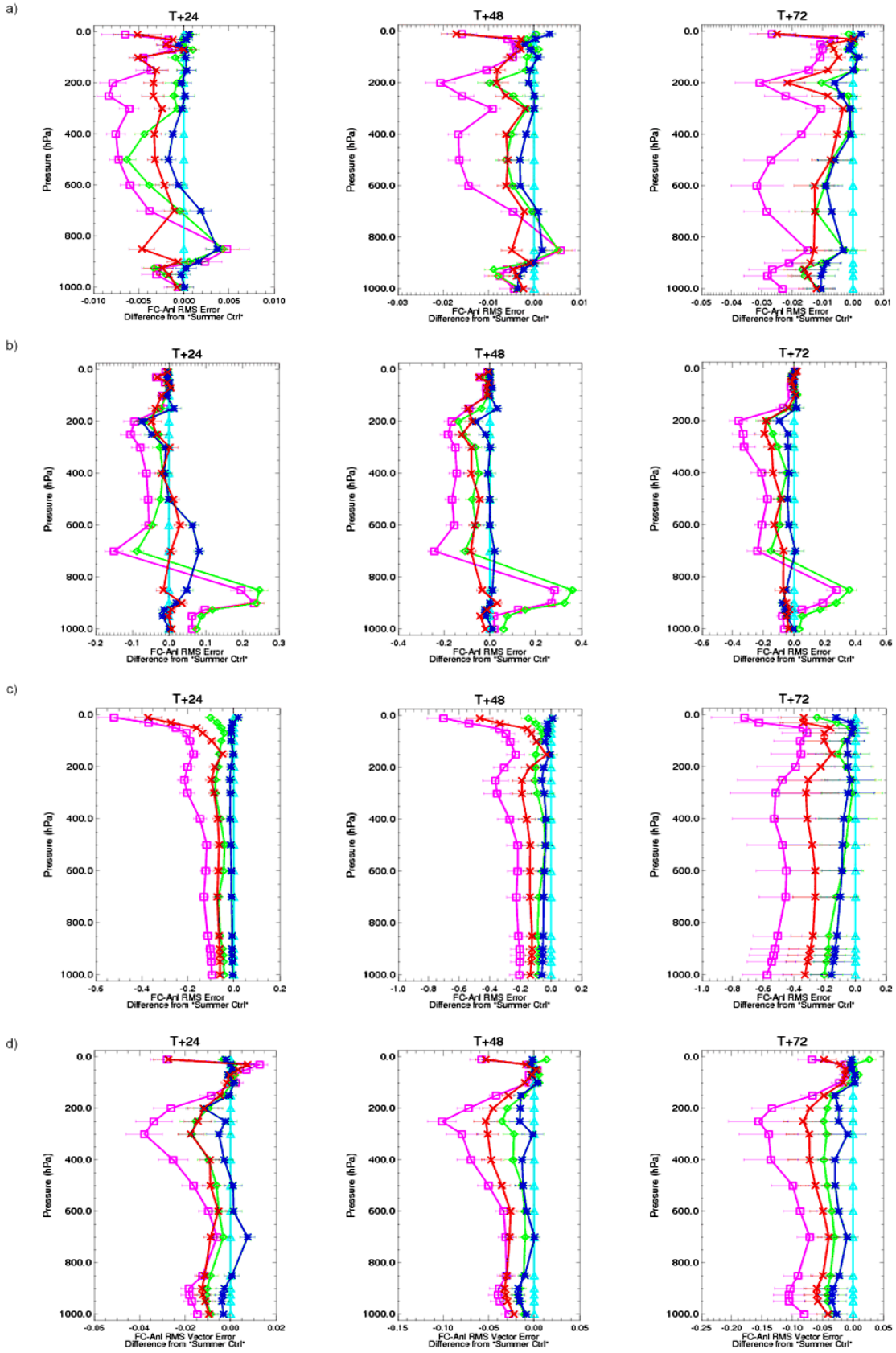

*Figure 13: Profiles show the changes in RMS errors in a) temperature b) relative humidity, c) geopotential height, and d) wind (forecast - analysis) fields in the southern hemisphere from the temperature (red x), humidity (blue *), imager (green ◊), and unified (pink □) assimilation experiments, wrt the no-SSMIS control (pale blue Δ).*

Conclusion

A new orbital bias correction technique has been implemented within the Met Office's variational bias correction data assimilation system. It has been found successful in mitigating the orbital biases for each of the F17, F18 and F19 SSMIS instruments. Data quality assessments showed the standard deviation of the SSMIS innovations (C-B) to be lower and hence better than those of the equivalent AMSU-A/ATMS temperature sounding and AMSR-3 imager innovations. The humidity sounding data were slightly worse than those of MHS/AMSU-B. NWP data assimilation experiments were carried out utilizing data from two SSMIS instruments, F17 and F18. The impact of assimilating temperature sounding, humidity sounding and imager data were trialled separately. However, the best performance was gained by assimilating the full complement of SSMIS channels. The assimilation of the SSMIS observations was shown to be particularly beneficial to the southern hemisphere temperature, geopotential heights and winds forecast fields. Consequently, the improved data from the SSMIS F17 and F19 instruments is due to be included in the Met Office's latest operational upgrade as of March 2016.

References

Booton, A, Bell, W, Atkinson, N, 2014, 'An improved bias correction for SSMIS', *Proceedings of the nineteenth International TOVS Study Group conference*, Available from https://cimss.ssec.wisc.edu/itwg/itsc/itsc19/program/papers/10_03_booton.pdf